

Cardiotoxicity Assessment through a Polymer-Based Cantilever Platform: An Integrated Electro-Mechanical Screening Approach

Pooja P. Kanade, Nomin-Erdene Oyunbaatar, Jongyun Kim, Bong-Kee Lee, Eung-Sam Kim, and Dong-Weon Lee*

Preclinical drug screening for cardiac toxicity has traditionally relied on observing changes in cardiomyocytes' electrical activity, primarily through invasive patch clamp techniques or non-invasive microelectrode arrays (MEA). However, relying solely on field potential duration (FPD) measurements for electrophysiological assessment can miss the full spectrum of drug-induced toxicity, as different drugs affect cardiomyocytes through various mechanisms. A more comprehensive approach, combining field potential and contractility measurements, is essential for accurate toxicity profiling, particularly for drugs targeting contractile proteins without affecting electrophysiology. However, previously proposed platform has significant limitations in terms of simultaneous measurement. The novel platform addresses these issues, offering enhanced, non-invasive evaluation of drug-induced cardiotoxicity. It features eight cantilevers with patterned strain sensors and MEA, enabling real-time monitoring of both cardiomyocyte contraction force and field potential. This system can detect minimum cardiac contraction force of $\approx 2 \mu\text{N}$ and field potential signals with $50 \mu\text{m}$ MEA diameter, using the same cardiomyocytes in measurements of two parameters. Testing with six drugs of varied mechanisms of action, the platform successfully identifies these mechanisms and accurately assesses toxicity profiles, including drugs not inhibiting potassium channels. This innovative approach presents a comprehensive, non-invasive method for cardiac function assessment, poised to revolutionize preclinical cardiotoxicity screening.

urgent need for more advanced and reliable methods to assess cardiac toxicity in drugs.^[1] More than 2000 medications introduced to the market have been found to adversely affect the heart. Moreover, a study examining drugs pulled from the market between 1990 and 2010 revealed that nearly 19% were removed due to severe cardiac side effects.^[1] Bringing a new drug to market requires a substantial median investment of \$1.14 billion.^[2] Given these stakes, evaluating potential drugs for cardiotoxicity is essential in reducing health risks and safeguarding consumers.

The International Conference of Harmonization (ICH) E14 guideline in 2005 and the subsequent Comprehensive in-vitro Proarrhythmia Assay (CiPA) initiative recommended approaches for preclinical screening of drug-induced cardiac toxicity. These approaches focused on understanding the electrophysiological changes in cardiomyocytes caused by drugs.^[3–5] The methods involved measuring the cardiac action potential using either the complex and invasive patch clamp or the non-invasive microelectrode array (MEA) to assess extracellular field potential.^[6–10] While MEA is favored over patch clamp for drug screening due to its simplicity and ability

for long-term assessment,^[11–13] the methods used so far mainly assessed changes in cardiac ion channels, placing emphasis on electrophysiological markers.^[14–17] It is worth reconsidering the

1. Introduction

Drug-induced cardiotoxicity remains a significant reason for withdrawing many drugs from the market, highlighting the

P. P. Kanade, N.-E. Oyunbaatar, J. Kim, B.-K. Lee, D.-W. Lee
School of Mechanical Engineering
Chonnam National University
Gwangju 61186, South Korea
E-mail: mems@jnu.ac.kr

P. P. Kanade, N.-E. Oyunbaatar, J. Kim, D.-W. Lee
Advanced Medical Device Research Center for Cardiovascular Disease
Chonnam National University
Gwangju 61186, Republic of Korea

E.-S. Kim
Department of Biological Sciences
Chonnam National University
Gwangju 61186, Republic of Korea
D.-W. Lee

Center for Next-Generation Sensor Research and Development
Chonnam National University
Gwangju 61186, Republic of Korea

 The ORCID identification number(s) for the author(s) of this article can be found under <https://doi.org/10.1002/sml.202311274>

DOI: 10.1002/sml.202311274

conventional belief that prolongation of field potential duration (FPD) or action potential duration (APD) is solely a result of potassium channel blockage. FPD prolongation can also arise from calcium channel activation or the simultaneous modulation of multiple ion channels. Some examples are Bay K-8644, which is a calcium channel activator, and Ranolazine, which is a multiple ion channel modulator.^[18,19] Additionally, many drugs target various proteins in cardiomyocytes that may have minimal impact on electrophysiology.^[20,21] Given that arrhythmia and the life-threatening Torsades de Pointes (TdP) primarily result from the reactivation and re-release of calcium ions during diastole, assessing contractile profiles alongside field potential measurements can offer valuable insights into proarrhythmic activities.^[22,23]

The force of contraction in muscle cells is governed by the process of excitation-contraction coupling, a crucial physiological mechanism that bridges the gap between electrical signals and mechanical contraction. This process is initiated by electrical impulses that lead to the release of calcium ions from the sarcoplasmic reticulum into the cytoplasm. The interaction of calcium with various contractile and regulatory proteins, facilitated by membrane pumps and mitochondria, ultimately triggers muscle contraction.^[24–26] This suggests that relying solely on electrophysiology to evaluate ion channel activity is insufficient for assessing drug-induced toxicity. Hence, a more reliable approach for identifying drug mechanisms and screening for cardiac drug toxicity involves a combined and simultaneous measurement platform that assesses both field potential and contractility. While standalone field potential measurements may lack certain proarrhythmic markers needed for predicting drug toxicity, integrating contractility measurements with electrophysiology can enhance the accuracy of proarrhythmic prediction. Currently, there is a lack of experimental evidence proving simultaneous measurement of electrophysiology and contractility using a single device. There are only a few reports available on the combined measurement of these parameters using MEA technology in conjunction with other mechanophysiological methods. For example, some studies have paired MEA with either invasive force measurement techniques, such as atomic force microscopy,^[27,28] or non-invasive force measurement techniques like video microscopy^[29] and impedance measurement,^[30–35] employing load cells,^[36] diaphragms,^[37] and cantilevers.^[38,39] However, the methods used so far suffer from certain key limitations. For instance, video microscopy methods require additional signal processing time for image analysis as well as measuring only the contractility of a single tissue sample. While impedance-based methods can measure the contractility of cardiac tissue, they cannot measure actual contractile force and employ high-frequency AC signals that can interfere with the simultaneous measurement of contractility and field potential. The load cell technique is a complex apparatus and is not suitable for long-term drug screening. Additionally, the PDMS diaphragm setup studied different cells for contractile and field potential measurement since the MEA was patterned outside the diaphragm. Techniques that employ cantilevers as substrates are increasingly recognized for their ability to measure cardiac contraction forces at the tissue level in a non-invasive manner. Moreover, these methods facilitate the integration of MEAs onto the cantilever surface, allowing the simultaneous evaluation of the field potential of car-

diac cells. PDMS cantilevers with integrated strain sensors coupled to MEA utilized spray printing and shadow masks to fabricate the strain sensor and MEA made of carbon nanoparticles.^[38] Additionally, an SU-8-based cantilever that detects displacement with an optical signal was combined with a gold-based MEA.^[39] However, cantilever-based devices developed so far face several challenges that hinder their wider application. For example, the PDMS cantilever required the use and optimization of carbon nanoparticles to achieve a high gauge factor, as the strain change was measured using change in resistance. The sensor fabrication method also poses serious problems in signal reproducibility. In the case of the SU-8 cantilever, the optical method used to measure cantilever displacement for contraction force assessment limited the potential for high-throughput drug screening. Furthermore, there is a desire to incorporate functional materials onto the cantilever substrate, as they have proven effective in enhancing the maturation of cardiomyocytes without the need for external electrical or mechanical stimulation.^[40] However, such materials can lead to bending of the polymer cantilever and the reflective area used for optical contractile measurements. Therefore, there is a pressing need for a reliable and comprehensive measurement system that allows for the comparison of tissue-level contraction force with field potential and better replicates *in vivo* conditions.

In this paper, we present an innovative multifunctional biomedical platform designed for the simultaneous measurement of electrophysiological and contractile properties of cardiomyocytes. This platform utilizes MEAs in conjunction with strain sensors integrated onto eight conductive cantilevers, enabling effective drug toxicity screening. The contraction force of cardiomyocytes is assessed by utilizing Wheatstone bridge in half-bridge configuration incorporated onto these cantilevers, while electrophysiological activity is measured using the integrated MEAs. Furthermore, we have integrated microgrooves and a conductive layer onto the 8 cantilevers, which serve to enhance the maturation, alignment, and connectivity of cardiac tissue—an essential aspect for reliable drug screening. A custom-made platform was developed with a home-made signal conditioning unit (SCU) for the strain sensor. Initially, we conducted sensitivity characterizations of both the strain sensors and the MEAs. Subsequently, our platform with the cantilever-device arrays was successfully employed to simultaneously measure field potentials and contractility in neonatal rat ventricular myocytes (NRVM). Using six different drugs, each with varying mechanisms of action (as detailed in Table S1, Supporting Information), we demonstrated the impact of these distinct mechanisms on field potential and contractile parameters. This highlights the necessity of a dual-measurement platform for comprehensive and dependable drug toxicity screening.

2. Results

2.1. Development of the Multifunctional Cantilever-Based Device

The proposed device for measuring contractility and field potential simultaneously involves a cantilever, which is equipped with a strain sensor at fixed ends to measure the contractile force of cardiomyocytes. Additionally, eight microelectrodes are also integrated on the cantilever to record the duration of the field

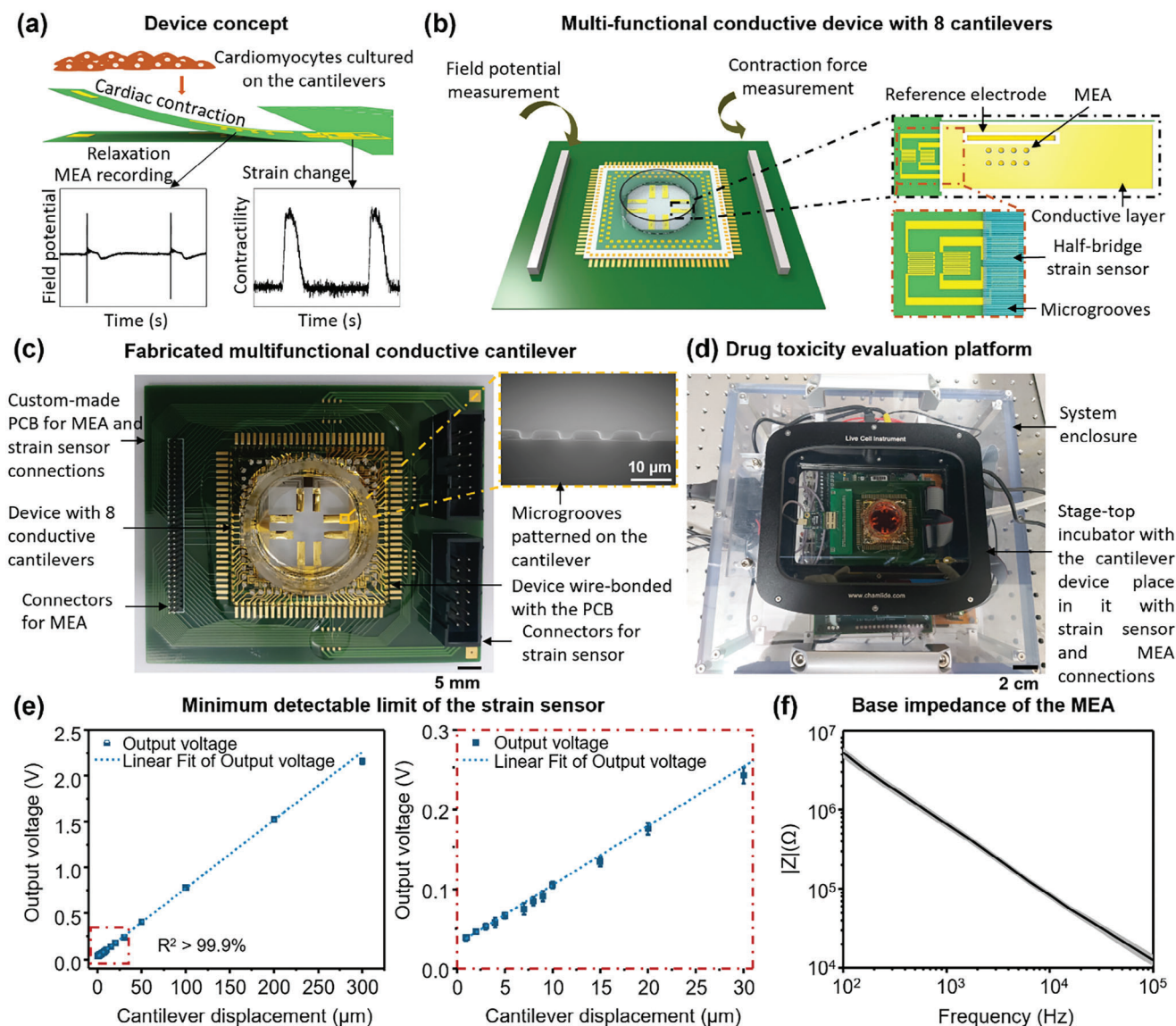


Figure 1. a) Schematic of the concept of simultaneous measurement of contractility and field potential using strain sensor and MEA on cantilever, b) schematic of the designed 8-cantilever device, with the enlarged schematic showing positions of MEA, reference electrode and strain sensor in the half Wheatstone bridge configuration, c) photo of the fabricated device bonded with a custom-made PCB, d) photo of the platform designed for drug toxicity screening using contractile and field potential assessments, e) sensitivity test of the strain sensor to detect minimum detectable displacement, f) assessment of the base impedance of MEA.

potential. Cardiomyocytes cultured on the cantilever proliferate and form a tissue layer. The cyclical contractions and relaxations of the cardiac tissue induce deflections of the cantilever, resulting in the change of tensile strain at the fixed end. The integrated strain sensor arranged in a half-bridge configuration on the cantilever continuously records the contractile behaviors of the cardiac tissue. The concept is illustrated schematically in **Figure 1a**.

The multifunctional cantilever-based device consists of eight polymer cantilevers made of SU-8, as shown in **Figure 1b**. SU-8 has a spring constant of ≈ 2.5 GPa.^[41] To achieve a spring constant of 15 mN m^{-1} (as calculated using Equation S1 in the Supporting Information), the dimensions of each cantilever were maintained at $6 \text{ mm} \times 2 \text{ mm} \times 14 \text{ μm}$, respectively. The enlarged

schematic in **Figure 1b** illustrates the positions of the microelectrodes, reference electrode, and strain sensor on the SU-8 cantilever. Two resistors from the strain sensor were patterned outside the cantilever on the device's body. These sensors, patterned using Ti/Au, were designed to have a resistance of 120 Ω each. **Figure S1a** (Supporting Information) displays an image of the cantilever with sensors before an isolation layer was applied. The isolation layer was subsequently patterned over the sensors to effectively isolate the strain sensor from the cardiomyocytes and culture media. It also created an open area for the MEA with a diameter of 50 μm . This diameter was chosen to ensure that the base impedance fell within an acceptable range for field potential measurements. **Figure 1b** illustrates the microgroove layer,

featuring 3 μm width and 3 μm spacing, as well as a Ti/Au conductive layer patterned on the isolation layer. The microgrooves were designed to provide topographical stimulation and alignment for the cardiomyocytes, while the conductive layer was patterned to enhance the expression of Connexin-43 protein within the tissue. The cantilever devices patterned on the 4-in Si wafer is presented in Figure S1b (Supporting Information). A total of 32 cantilevers could be fabricated on the wafer. As shown in the enlarged image in Figure S1b (Supporting Information), the conductive layer covered the entire surface except for the MEA areas. The released cantilever devices were thermally bonded to the patterned glass (Figure S1c, Supporting Information). This allowed for the manual connection of metal contacts on the cantilever body to the patterned contacts on the glass using conductive epoxy. The cross-section of the released cantilever was confirmed using a field emission scanning electron microscope (FE-SEM), which revealed uniform patterning of the microgrooves on the cantilever (Figure 1c). Since flexible materials such as SU-8 cannot be wire-bonded directly to the PCB, the glass plate was employed as the basis for cell culture and for joining MEA and strain sensors to the PCB by wire bonding (Figure S1d, Supporting Information; Figure 1c).

2.2. Drug Toxicity Evaluation Platform and its Characterization

2.2.1. Integration and Configuration of the Multifunctional Platform

A multifunctional platform designed for simultaneous assessment of cardiac field potential and contractility has been developed for our cantilever-based device. As illustrated in Figure 1d, this platform is capable of measuring both the field potential and contraction force of cultured cardiomyocytes. The device was kept in a stage-top incubator (Figure S2a, Supporting Information) and was connected to the allied SCU for measurement in the system enclosure (Figure S2b, Supporting Information). The enclosure consisted of three layers. The bottom-most layer comprised of the AC-DC power supply, that supplied power to the strain sensor and MEA SCUs, and data acquisition unit (DAQ) that was connected to a computer (Figure S3a, Supporting Information), while the home-made strain sensor SCU was placed in the second layer (Figure S3b, Supporting Information). The SCU was made of individual filter and amplifier circuits for the eight strain sensors. The filter circuits were the 3rd order active filters with a cut-off frequency of 16 Hz, while the amplifier used was an instrumentation amplifier. The top layer of the system consisted of the commercial MEA USB interface board (Figure S3c, Supporting Information).

2.2.2. Characterization of the Strain Sensor

The strain sensor was configured in a half-bridge arrangement within the Wheatstone bridge setup. It featured two resistors, R_1 and R_4 , positioned at the fixed end of the cantilever, while R_2 and R_3 were formed on the fixed body outside the cantilever (Figure S1a, Supporting Information). This configuration allowed us to measure the deflection of the cantilever by detecting changes in the output potential of the strain sensor. In order to determine the

smallest detectable displacement that the strain sensor could reliably capture, an experiment was conducted measuring the displacement of the cantilever on an automated Z-stage. A needle was used to control and manipulate the displacement of the free end of the cantilever, and the Z-stage controller provided precise control over the magnitude of cantilever displacement. All the resistors within the strain sensor were patterned to ensure their resistances matched. As a result, the initial output voltage of the strain sensor, referred to as SCU, remained below 0.5 mV when using a 1x gain setting. Consequently, we were able to maintain the amplification of the instrumentation amplifier at 10 000x without any issues. Figure 1e illustrates the relationship between the displacement of the cantilever and the corresponding output voltage of the strain sensor, with a 10 000x amplification applied. Cantilever displacement was applied from 300 μm and was reduced until it was undetectable. The smallest detectable displacement we were able to record was 900 nm. Any displacements smaller than 900 nm were indistinguishable from the baseline noise. It is worth noting that the minimum detectable displacement of 900 nm corresponds to a contraction force of 2.1 μN exerted by the entire cultured tissue, as the cantilever displacement is directly linked to the cardiac contraction force, as shown in Figure S4 (Supporting Information).^[42,43]

The long-term stability of the strain sensor's baseline was rigorously evaluated to ascertain the reliability of the sensor for prolonged drug toxicity assessments. Figure S5a (Supporting Information) illustrates the baseline performance of the sensor in air, whereas Figure S5b (Supporting Information) depicts the baseline in a culture medium under a 10 000x amplification. Despite both baselines maintaining stability throughout the observation period, a notable discrepancy was observed in the noise levels of the output voltage. Specifically, the noise level in the culture medium exceeded that in air, potentially attributable to motion artifacts within the medium, which could induce minor displacements in the cantilever. However, these factors notwithstanding, the sensor's baseline demonstrated consistent stability over an extended duration.

To further elucidate the performance of the strain sensor, its output voltage was analyzed in relation to temperature variations. The experimental setup involved placing the sensor in a stage-top incubator and methodically decreasing the temperature from 40 $^{\circ}\text{C}$ to 25 $^{\circ}\text{C}$ in 5 $^{\circ}\text{C}$ increments. As depicted in Figure S5c (Supporting Information), the sensor's output voltage exhibited a linear relationship with temperature changes. Notably, the output voltage registered higher in air compared to the culture medium. This discrepancy is attributed to the initial bending of the SU-8 polymer cantilever in the culture medium, which imparted an initial strain on the sensor. The observed linearity was pronounced, with a coefficient of determination (R^2) exceeding 98.1% in air and 99.8% in culture medium. Such linearity in the sensor's response to temperature changes further corroborates the reliability of the sensor for precise measurements.

2.2.3. Characterization of the base Impedance of MEA

The base impedance of the MEA was evaluated to comprehend the noise attributes of the field potential signal. Impedance spectrum measurements were taken from 10³ to 10² Hz, as depicted

in Figure 1f, with the help of the 3-electrode method. Within this range, the spectrum displayed an almost linear pattern, and the impedance stood at $859.4 \pm 142.1 \text{ k}\Omega$ at 1 kHz. Given its alignment with the acceptable parameters for a 50 μm diameter Au MEA, it was selected for this study.

2.3. Protein Expression of the Cultured Cardiomyocytes

After characterizing the cantilever-based device and platform, NRVM were cultured on the cantilevers at a density of 1000 cells mm^{-2} . All the experiments were performed following the protocol approved by the Animal Ethics Committee of Chonnam National University in accordance with the Principles of Laboratory Animal Care and specific national laws (license number: CNU IACUC-YB-2022-29). The cardiomyocytes were transferred to the incubator after cell culture and maintained at 37 °C under 5% CO_2 .^[39,40] Culture medium was changed once every two days. The detailed NRVM culture protocol is described in supplementary information. During the initial three days, the cardiomyocytes adhered to the substrate, culminating in a monolayer formation.^[42] The incorporation of a gold layer on the cantilever's surface posed complexities in analyzing protein expression through immunocytochemical (ICC) staining. Consequently, Western blotting was adopted for this analytical purpose. Figure S6 (Supporting Information) displays the Western blot results obtained from NRVM under various conditions: control, flat SU-8, and SU-8 integrated with a conductive layer. The data revealed elevated levels of protein expression, marked by significant increases in α -actinin, connexin 43 (Cx43), troponin-c, and vinculin. These findings suggest that the Au metal layer on the SU-8 cantilever plays a pivotal role in facilitating electrophysiological maturation essential for in vitro cardiomyocyte tissue engineering. Moreover, the synergistic effect of the conductive substrate and the microgrooved topography was observed to enhance the electrical connectivity among cardiomyocytes, leading to increased cantilever displacement. Therefore, the electroconductive substrate emerged as a critical factor in promoting the maturation of cardiomyocytes.

2.4. Comparative Analysis of Cardiac Contractility using Strain Sensor Metrics and Cantilever Displacement

We prepared the custom-made PCB that can simultaneously measure contractility from 8 cantilevers, using which the minimum detectable cardiac contraction force was 2.1 μN . The next step was to understand the rise and decay slopes of the contractile profile. The contractile patterns of cardiomyocytes were assessed both electrically and optically. The strain sensor output voltage was compared with the cantilever displacement measured using the laser vibrometer. The measurements carried out on day 8 after cell culture are shown in Figure S7 (Supporting Information). The electrical and optical contractile patterns were similar to each other, with the rise and decay times matching precisely. Therefore, using strain sensor output for contractility using our custom-made SCU did not result in loss of information and could be used reliably.

2.5. Simultaneous Assessment of Cardiac Contractility and Field Potential

After evaluating the contractile profile, field potential, and contractility were measured concurrently using our system. Figure 2a,b displays these simultaneous measurements conducted by the eight cantilevers. Each cantilever had cardiac tissue forming a monolayer, which generated sufficient contraction force to bend the cantilever, creating strain. Although contained in the same culture medium, cardiac tissue of each cantilever was isolated, resulting in asynchronous beating (Figure 2a). Field potential signals were simultaneously recorded from 64 microelectrodes—eight per cantilever. Figure 2b presents four out of the eight field potential readouts from each cantilever. Most signals were distinct with a baseline within the acceptable range of $\approx \pm 22 \text{ }\mu\text{V}$. The field potential typically showed an initial sharp negative deflection followed by a positive swing and then a slight negative dip before returning to the baseline. This negative spike indicates the start of the action potential, mainly due to the rapid influx of Na^+ ions through the cardiomyocyte membrane. This is followed by an inward Ca^{2+} current and the release of Ca^{2+} from the sarcoplasmic reticulum. The final peak in the field potential coincides with the end of the action potential repolarization phase, which involves K^+ channels. FPD is measured from the start of the negative deflection to the next positive or negative peak, based on the signal's contour. Cardiac contraction is closely tied to the electrical activity of cardiomyocytes. As Ca^{2+} enters the cardiomyocyte, it triggers a significant release of Ca^{2+} from the sarcoplasmic reticulum. The attachment of Ca^{2+} to troponin leads to sarcomere contraction. During relaxation, Ca^{2+} is reabsorbed into the sarcoplasmic reticulum and expelled from the cardiomyocytes. This cycle lasts longer than the field potential, indicating that the cardiomyocyte contraction process continues beyond the FPD.

Despite the asynchronous beating of the cantilevers, the number of cardiomyocytes cultured on each was comparable, which resulted in a similar range of contraction forces exerted on the cantilevers. Figure 2c illustrates the analysis of the contractile activity for each cantilever. A slight variation in contractility was observed, ranging from 243 to 258 mV; however, this difference was not statistically significant, allowing us to disregard it. Parallel evaluations were conducted for FPD as shown in Figure 2d, and the beat rate as depicted in Figure 2e. The FPD showed a variation from an average of 173 ms up to 178 ms across the eight cantilevers, while the beat rate fluctuated between an average of 0.58 and 0.63 Hz which were in the acceptable range.^[44] These observed differences in both parameters among the cantilevers were also statistically insignificant, which further substantiates the dependability of our cell culture method using this device.

2.6. Platform Used for Drug-Induced Toxicity Screening

After confirming protein expression in the cultured cardiomyocytes, as well as their electrical and mechanical functions, our platform was employed to examine the alterations in electrophysiology and contractility upon the introduction of cardiotoxic drugs. Six drugs, each with a distinct mechanism of action, were selected for this study. Two of the drugs targeted the Ca^{2+} chan-

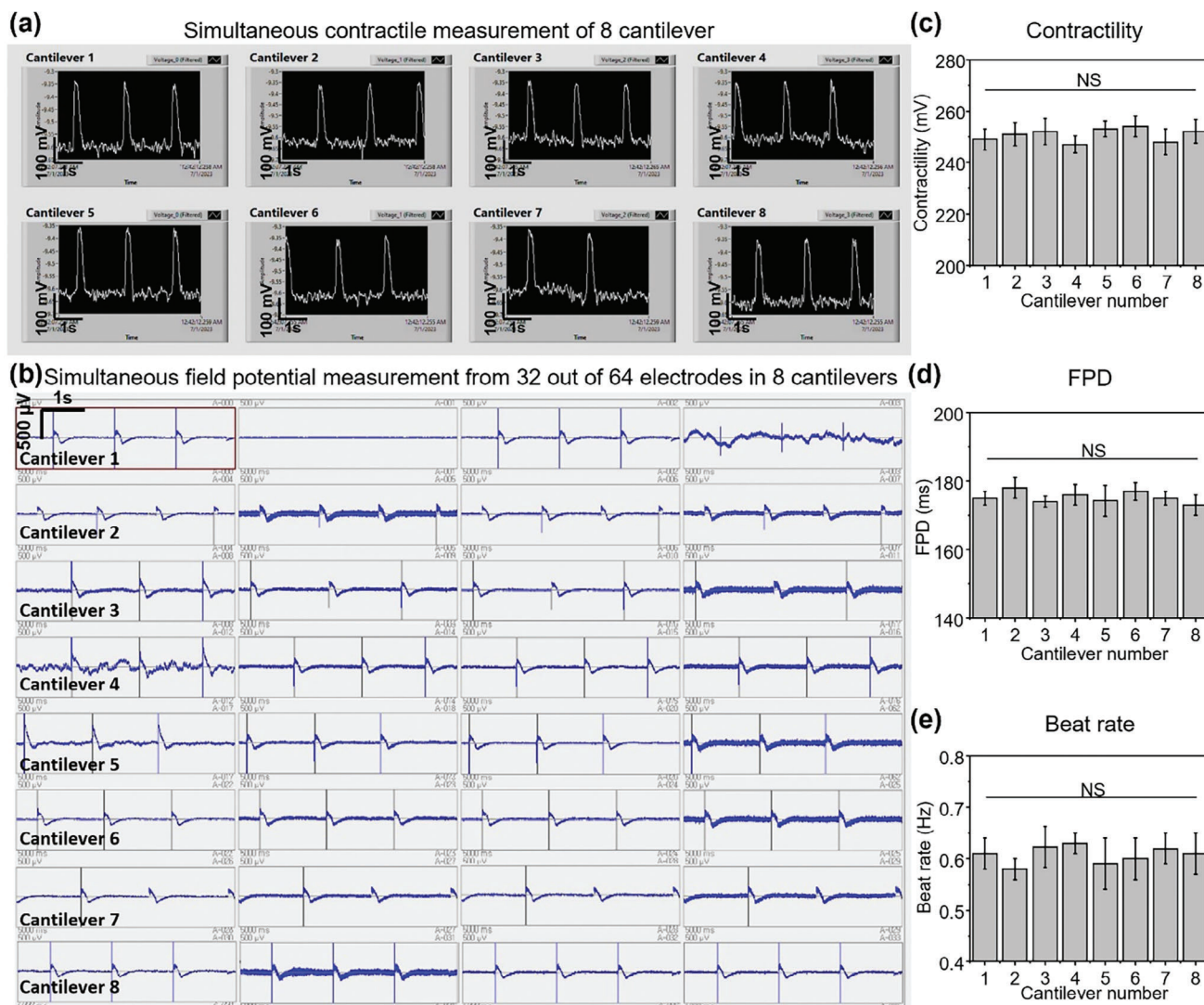


Figure 2. a) Simultaneous measurement of strain sensor output voltage of all the 8 cantilevers along with b) simultaneous measurement of field potential from 32 microelectrodes out a total of 64 microelectrodes. The analyses of variability in c) contractility, d) FPD and e) beat rate for 8 cantilevers are carried out.

nels (Nifedipine, a Ca^{2+} blocker, and Bay K-8644, a Ca^{2+} activator), two influenced other essential ion channels (Astemizole, a K^{+} channel blocker, and Quinidine, a Na^{+} channel blocker), and the remaining two affected alternative pathways in cardiomyocytes (Blebbistatin, a myosin inhibitor, and Isoproterenol, a beta-adrenoceptor).

The first drug tested was nifedipine, a class IV calcium ion channel blocker,^[45] known for its negative chronotropic (decreased beat rate) and negative inotropic (reduced contractility) impacts on cardiomyocytes.^[46] The drug was administered in ascending concentrations from 1 nM to 10 μM . **Figure 3a** shows the characteristic changes in contractility and field potential at both control levels and with 50 nM nifedipine. There was a noticeable decrease in contraction force following drug addition, and the beat rate also declined in a concentration-dependent fashion, as mirrored in the field potential readings. With increasing drug concentrations, the FPD decreased, as shown by the su-

perimposed curves in **Figure S8** (Supporting Information), with the repolarization peak shifting earlier. At a higher concentration of 1 μM , there was a significant reduction in contraction force (**Figure S9a**, Supporting Information), and the field potential signal weakened with an extremely small FPD (**Figure S9b**, Supporting Information). The primary measures of field potential and contractility, namely the corrected field potential duration (FPDc), beat rate, and contractility, decreased notably at 50 nM to average factors of 0.81, 0.84, and 0.70, respectively, compared to control values. The field potential spike amplitude (FPA) also decreased, although this change was not statistically significant (**Figure 3b**). The field potential spike is mainly caused due to the change in the rate of depolarization of action potential, which results from the rapid influx of Na^{+} ions. Nifedipine did not directly affect the Na^{+} channel or block the channel activity; therefore, the FPA parameter was not significantly affected.

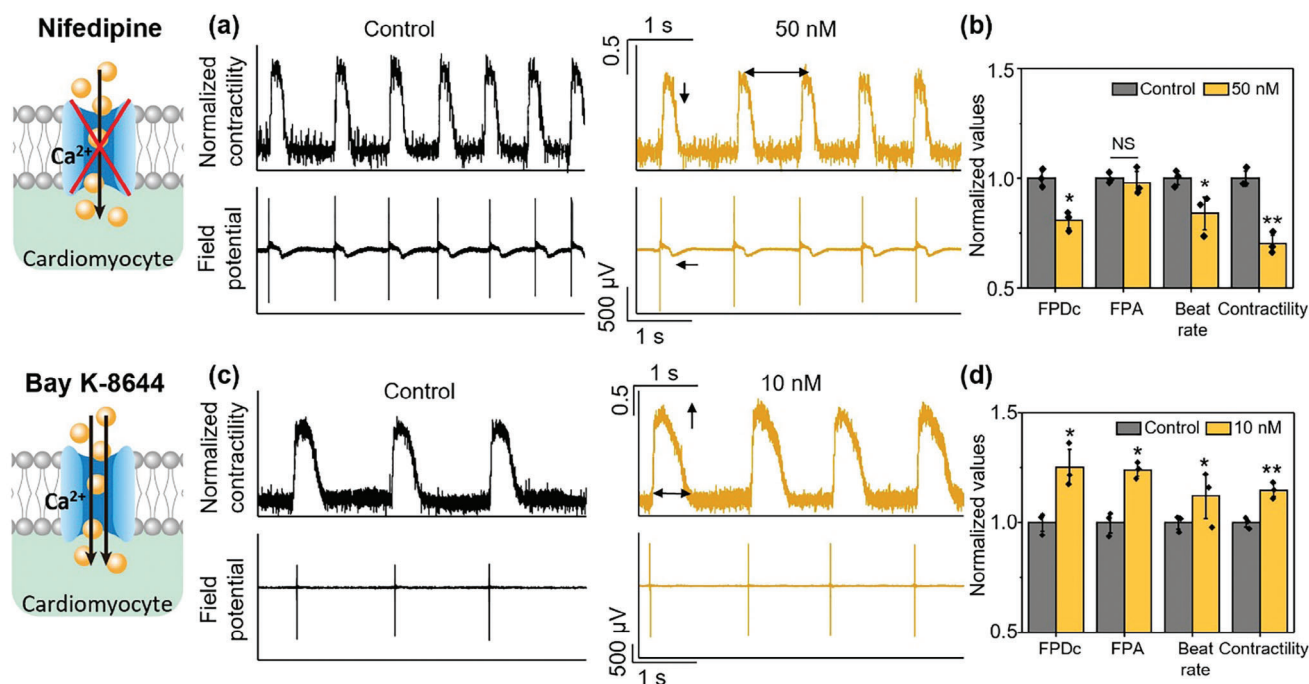


Figure 3. Effect of Ca^{2+} channel blocker and activator on contractility and field potential of cardiomyocytes. a) Contractility and field potential changes on addition of 50 nM Nifedipine with respect to control, b) analyses of change in corrected field potential duration (FPDc), field potential spike amplitude (FPA), beat rate and contractility, on addition of 50 nM Nifedipine, c) contractility and field potential changes on addition of 10 nM Bay K-8644 with respect to control, d) analyses of change in FPDc, FPA, beat rate and contractility, on addition of 10 nM Bay K-8644. Corrected field potential duration (FPDc) was calculated using Fredericia's formula ($\text{FPDc} = \text{FPD} (\text{interspike interval})^{-1/3}$). Analysis carried out from $n = 3$ biologically independent samples. Statistical significance of data was determined with the help of one-way ANOVA followed by Tukey's honest significant difference test, with significant differences defined by $*p < 0.05$ and $**p < 0.01$.

The second drug was Bay K-8644, a Ca^{2+} channel activator known to enhance the influx of Ca^{2+} and thus, increase the contraction force.^[47,48] An elevated Ca^{2+} level can extend the repolarization period, thereby prolonging the FPD. Bay K-8644 was applied in increasing concentrations from 1 nM to 1 μM . This drug was observed to induce a positive inotropic effect by increasing intracellular calcium concentration. Figure 3c presents the representative effects on contraction force and field potential at baseline and with 10 nM of the drug. At the 1 μM concentration, the cardiomyocytes exhibited arrhythmic activity resembling tachyarrhythmia, as shown in Figure S10 (Supporting Information).^[49] Figure 3d displays the variations in field potential and contractile parameters induced by Bay K-8644. In contrast to Nifedipine, Bay K-8644 led to an escalation in these parameters, showing an increase by a factor of 1.25 for corrected FPD (FPDc), 1.24 for field potential amplitude (FPA), 1.12 for beat rate, and 1.15 for contractility.

The third drug, Astemizole, is a K^+ channel blocker. It is associated with negative chronotropic and inotropic effects on cardiomyocytes, alongside an elongation of FPD.^[50,51] Astemizole was added in a stepwise sequence at concentrations ranging from 100 pM to 100 nM. Figure 4a illustrates the changes in contractility and field potential at baseline and with 10 nM of the drug. While the contraction force decreased slightly with an increase in concentration, this change was not statistically significant; however, the beat rate experienced a substantial reduction. The FPD showed an increase with higher concentrations, as evidenced in

Figure S11 (Supporting Information). At a concentration of 1 μM , TdP, a dangerous arrhythmia potentially leading to heart failure, was noted in the cardiomyocytes' beating patterns (Figure S12, Supporting Information). It is crucial to monitor the concentrations at which this condition arises. According to Figure 4b, the FPDc increased to 1.04 times the control value, whereas the beat rate and contractility diminished to 0.71 and 0.94 of the control values, respectively. The FPA experienced a slight increase, but this was not statistically significant.

The fourth drug tested was quinidine, a class Ia Na^+ channel blocker.^[52] This type of blocker also moderately inhibits the human ether-a-go-go (hERG) potassium channel, which can lead to an extended repolarization period.^[53] We exposed cardiomyocytes growing on the cantilever to quinidine at concentrations ranging from 10 nM to 10 μM . Figure 4c displays the typical changes in contractility and field potential at baseline and with 500 nM of quinidine. The contraction force showed a minor decrease as the concentration increased, and the beat rate also declined. At 10 μM , TdP was observed in the cardiomyocyte beat patterns (Figure S13, Supporting Information). Regarding the field potential signal, hERG channel inhibition resulted in a prolonged FPD, while Na^+ channel blockage led to a reduced spike amplitude. Figure S14 (Supporting Information) illustrates the dose-dependent shift to the right in the repolarization peak of the field potential (Figure S14a, Supporting Information) and a reduction in spike amplitude (Figure S14b, Supporting Information). Figure 4d indicates that hERG blockade caused a 1.07-fold

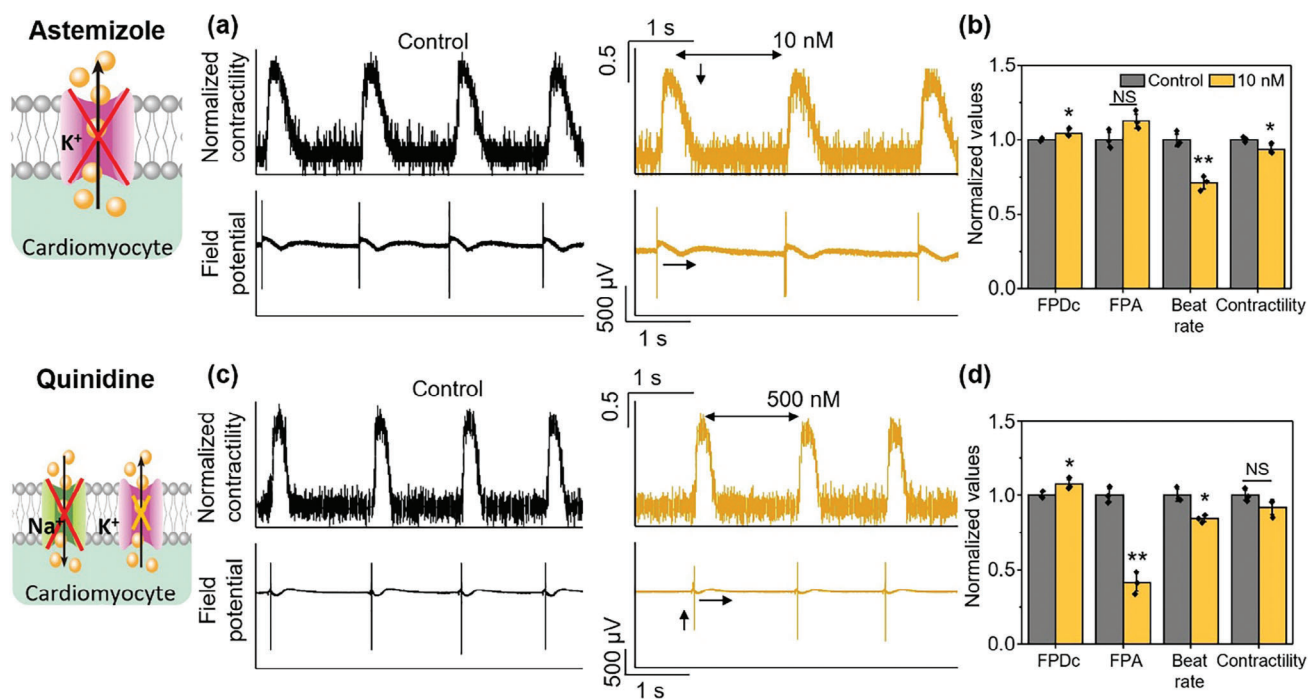


Figure 4. Effect of other ion channel blockers on contractility and field potential of cardiomyocytes. a) Contractility and field potential changes on addition of 10 nM Astemizole with respect to control, b) analyses of change in corrected field potential duration (FPDc), field potential spike amplitude (FPA), beat rate and contractility, on addition of 10 nM Astemizole, c) contractility and field potential changes on addition of 500 nM Quinidine with respect to control, d) analyses of change in FPDc, FPA, beat rate and contractility, on addition of 500 nM Quinidine. Corrected field potential duration (FPDc) was calculated using Fredericia's formula ($FPDc = FPD (\text{interspike interval})^{-1/3}$). Analysis carried out from $n = 3$ biologically independent samples. Statistical significance of data was determined with the help of one-way ANOVA followed by Tukey's honest significant difference test, with significant differences defined by $*p < 0.05$ and $**p < 0.01$.

increase in corrected FPD (FPDc), while Na^+ blockade resulted in a spike amplitude (FPA) decrease to 0.41 times the control value at 500 nM. The beat rate and contractility decreased to 0.84 and 0.92 of the control values, respectively.

Subsequently, Blebbistatin, a myosin II inhibitor, was evaluated.^[54] As an excitation-contraction decoupling agent, Blebbistatin primarily affects contraction without significantly altering the field potential. This drug was added to the cardiomyocytes with sequentially increasing concentrations of 10 nM, 100 nM, 500 nM, 1 μM , 5 μM , and 10 μM . Figure 5a shows the visual representation of contraction force and field potential at baseline and with 10 μM of Blebbistatin. The introduction of the drug did not affect the field potential, but the contraction force decreased to zero, and the cardiomyocytes ceased beating (Figure 5b). Electrophysiological parameters such as FPDc and FPA showed no significant changes.

The final drug was Isoproterenol, a beta adrenoceptor agonist.^[55] It activates β_1 and β_2 receptors, leading to an increased intracellular calcium current and, consequently, an augmented contraction force. Known for its positive chronotropic and inotropic effects, Isoproterenol was added in a sequence of concentrations from 10 nM to 100 μM . Figure 5c illustrates the changes in contractility and field potential at baseline and with 100 nM Isoproterenol, where a slight increase in contraction force and a significant rise in beat rate were observed. As detailed in Figure 5d, FPDc decreased to 0.68 times its control value, while

the beat rate and contractility rose to 1.53 and 1.09 times their control values, respectively. FPA remained largely unchanged.

We also assessed the drug toxicity and its effects on field potential and contractile parameters. Figure 6a examines the toxic effects of Nifedipine, showing a concentration-dependent reduction in FPDc with an IC_{50} of 50.16 nM, which is attributable to the inhibition of Ca^{2+} ions leading to earlier repolarization (Figure 6a1). As the contraction-relaxation duration is closely related to FPD, the corrected contraction-relaxation duration (CRDc) decreased with increasing drug concentration, with an IC_{50} of 318.6 nM (Figure S15a, Supporting Information). Cardiac contractility exhibited negative inotropy with an IC_{50} of 242.5 nM, and the beat rate displayed negative chronotropy with an IC_{50} of 511.3 nM. At higher concentrations, the contractile rise time lengthened, while the decay time shortened, potentially due to a slower beat rate and reduced calcium influx (Figure S15b, Supporting Information). In the case of Bay K-8644, an increase in calcium led to delayed repolarization and an extended FPD, although the prolongation did not conform to Hill's function, precluding calculation of the EC_{50} (Figure 6b1). Meanwhile, the contraction force saw an increase of up to 1.2 times in a dose-dependent manner following Hill's function, with an EC_{50} of 4.6 nM (Figure 6b2). The beat rate initially rose slightly, then surged by 4.5 times at a 1 μM concentration (Figure 6b3). It seems the CRDc trend mirrored that of the FPDc (Figure S16a, Supporting Information). These results suggest that at high

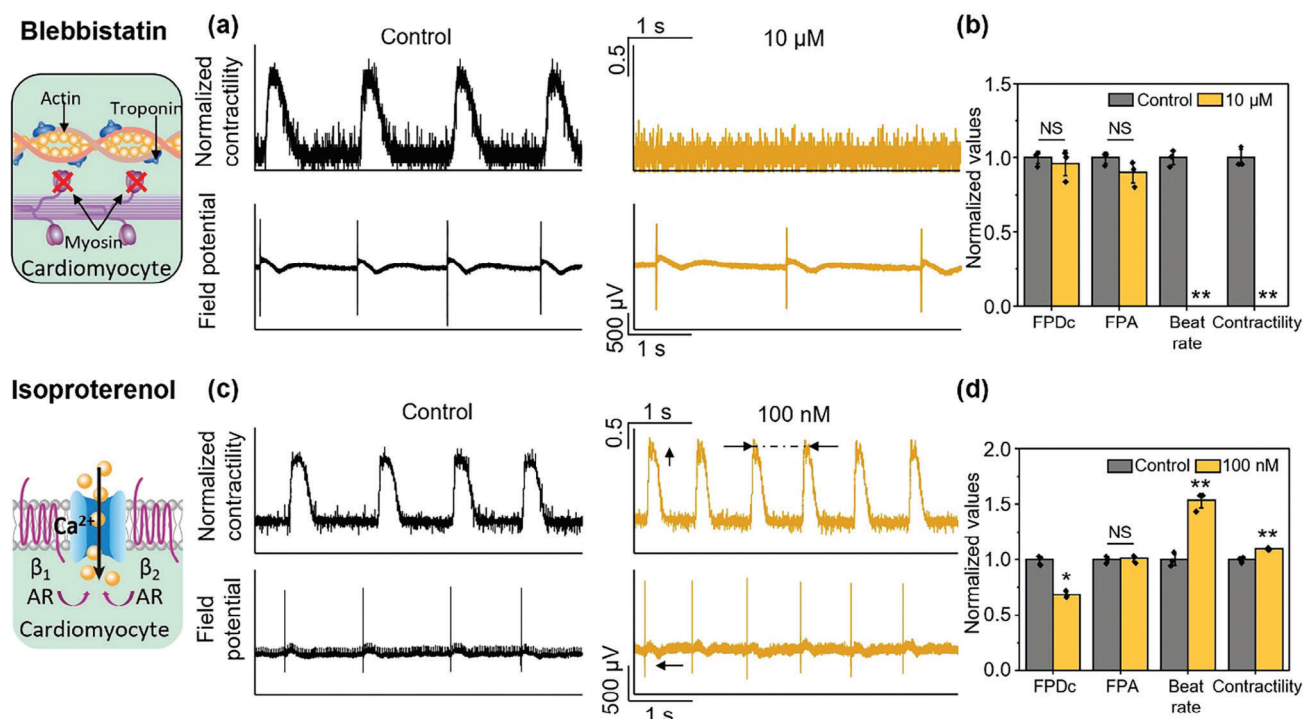


Figure 5. Effect of non-ion channel modulators on contractility and field potential of cardiomyocytes. a) Contractility and field potential changes on addition of 10 μM Blebbistatin with respect to control, b) analyses of change in corrected field potential duration (FPDc), field potential spike amplitude (FPA), beat rate and contractility, on addition of 10 μM Blebbistatin, c) contractility and field potential changes on addition of 100 nM Isoproterenol with respect to control, d) analyses of change in FPDc, FPA, beat rate and contractility, on addition of 100 nM Isoproterenol. Corrected field potential duration (FPDc) was calculated using Fredericia's formula ($FPDc = FPD \cdot (\text{interspike interval})^{-1/3}$). Analysis carried out from $n = 3$ biologically independent samples. Statistical significance of data was determined with the help of one-way ANOVA followed by Tukey's honest significant difference test, with significant differences defined by $*p < 0.05$ and $**p < 0.01$.

concentrations, calcium channels rapidly reactivate, triggering a swift release of calcium from the sarcoplasmic reticulum. The contractile parameters were also affected; the rise time shortened with an increasing beat rate, whereas the decay lengthened due to prolonged repolarization (Figure S16b, Supporting Information). Figure 6c (c1–c3) presents the toxicity analysis for the K^+ channel blocker Astemizole. The FPDc increased with an EC_{50} of 24.69 nM (Figure 6c1), and the CRDc also increased with an EC_{50} of 136.4 nM (Figure S17a, Supporting Information). The contraction force waned with an IC_{50} of 41.95 nM (Figure 6c2), while the beat rate decreased, not adhering to Hill's function of toxicity (Figure 6c3). The diminished contraction force upon adding the hERG channel blocker could be due to the protracted repolarization causing delayed calcium efflux. Although the total calcium content within the cardiomyocytes remained constant, the delayed efflux could result in weaker contractions and an extended CRD. For Astemizole, both the rise and decay times increased with higher concentrations (Figure S17b, Supporting Information). With the Na^+ channel blocker Quinidine, trends for both FPDc and FPA followed Hill's function, with an EC_{50} for FPDc at 836.1 nM (Figure 6d1) and an IC_{50} for FPA at 285.9 nM (Figure 6d2). Correspondingly, the CRDc altered with an IC_{50} of 1.713 μM (Figure S18a, Supporting Information). Quinidine also manifested negative chronotropy with an IC_{50} of 392.4 nM (Figure 6d3). The contraction force diminished to 0.78 times the control value at 10 μM, indicating negative inotropy (Figure S18b,

Supporting Information). The rise time increased slightly but not significantly, while the decay time lengthened due to the delayed closure of calcium channels caused by hERG blockage (Figure S18c, Supporting Information). Figure 6e (e1–e3) delineates the toxicity effects of Isoproterenol on various field potential and contractile parameters. The FPDc decreased but did not comply with Hill's function for inhibitory effects (Figure 6e1). The positive inotropy escalated with an EC_{50} of 17.93 nM (Figure 6e2), and the positive chronotropy rose with an EC_{50} of 192.8 nM (Figure 6e3). Initially, the CRDc diminished and then stabilized at higher drug concentrations (Figure S19a, Supporting Information). Both the contractile rise time and decay time decreased with higher drug doses (Figure S19b, Supporting Information). For Blebbistatin, while the FPD remained unaltered (Figure 6f1), the contraction force was concentration-dependent and decreased with an IC_{50} of 872.1 nM (Figure 6f2). The beat rate declined with an IC_{50} of 1.822 μM, at which point the cardiomyocytes ceased to beat (Figure 6f3).

3. Discussion

In this study, we have successfully developed a cardiac sensing system that demonstrates significant advancements over existing cantilever-based measurement platforms. The multifunctional nature of our system, capable of simultaneously measuring contraction force and field potential, sets a new standard in

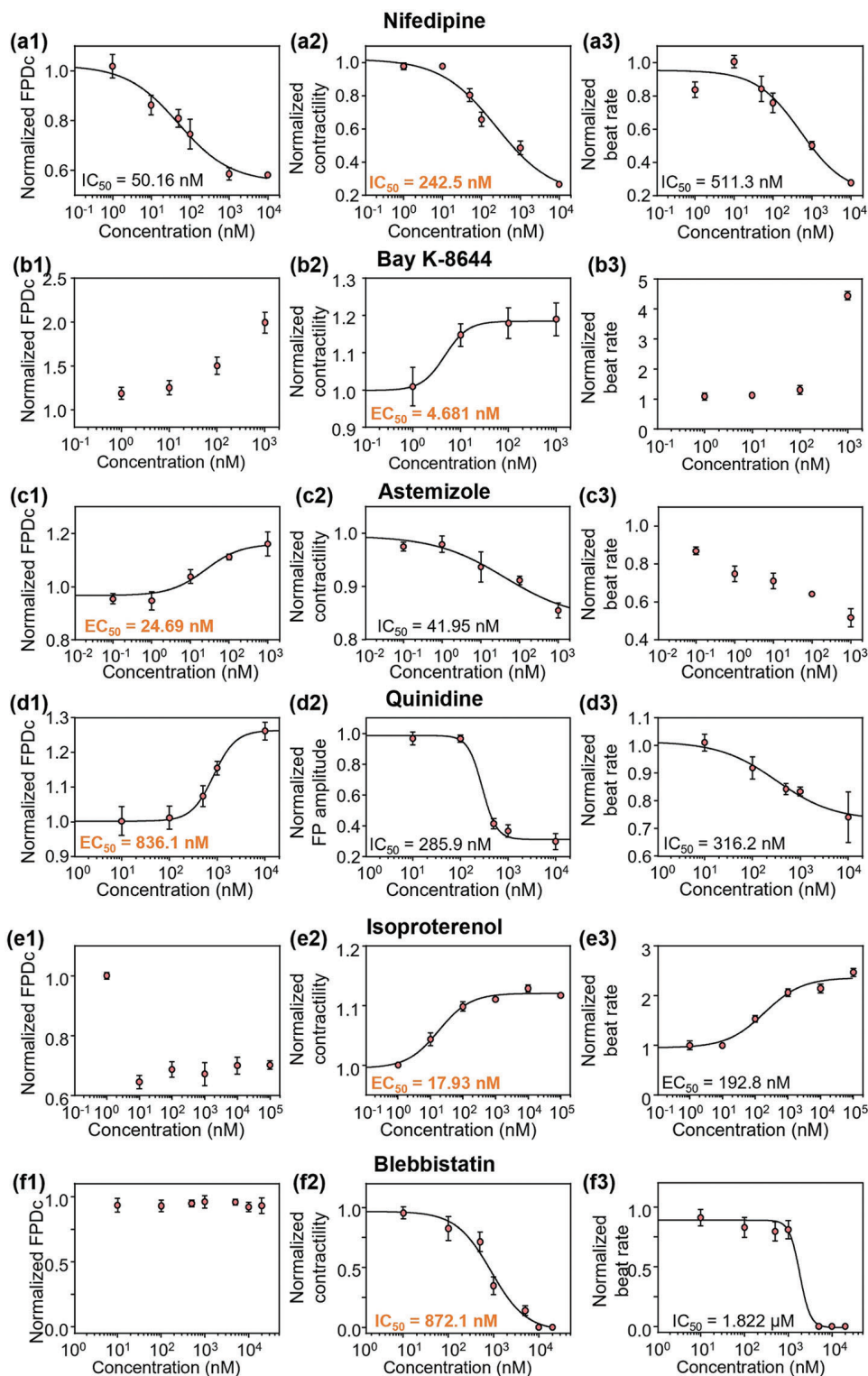


Figure 6. Drug toxicity screening results on (1) corrected field potential duration (FPDc), (2) normalized contractility/ normalized FP amplitude and (3) normalized beat rate, using our platform. Drugs used are (a1–a3) Nifedipine, (b1–b3) Bay K-8644, (c1–c3) Astemizole, (d1–d3) Quinidine, (e1–e3) Isoproterenol and (f1–f3) Blebbistatin. The half maximal toxicity values (IC_{50}) values in the drug toxicity analyses are calculated using the Hill's function. In each drug, the highlighted IC_{50} shows the key IC_{50} value. FPDc corrected using Fredericia's correction formula $FPDc = FPD (\text{interspike interval})^{-1/3}$. Drug toxicity screening analyzed using 3 biologically independent samples for each drug.

drug-induced cardiotoxicity screening. The utilization of 8 cantilevers in the system enhances the efficacy of drug screening, allowing for a more comprehensive and accurate analysis of cardiac tissue behavior. A key feature of our platform is its efficiency, simplicity, and reliability. The design of the Au-based strain sensor in the half-bridge configuration ensures robust performance and sufficient sensitivity without the need to enhance gauge factor. The use of the SU-8 cantilever arrays, combined with the strain sensor and MEA, not only simplifies the fabrication process via photolithography but also allows for scalability. This scalability is crucial in adapting the device for various research needs, making it a versatile tool in cardiac research. The size of the SU-8 cantilever-based device can be further reduced for higher throughput. Future work will focus on miniaturization of our device as well as development of a smart and portable platform for rapid drug toxicity screening. The potential of reusability of the miniaturized cantilever device would also be carefully assessed in the future as this work did not test the device reusability.

Moreover, the results from Western blot analysis highlight the role of microgrooves and the conductive layer in facilitating the maturation of cardiac tissue. This aspect of the design not only contributes to the physiological relevance of the study but also reinforces the applicability of the system in cardiac tissue research. While the opacity of the Au conductive layer on the cantilevers posed a challenge for observation under an inverted microscope, we successfully circumvented this issue by observing cantilever deflection. Furthermore, the use of an upright microscope offers an alternative method for tissue observation, effectively addressing the opacity challenge and negating it as a significant limitation. The uniform deflection observed across all cantilevers, attributed to the similar number and uniform distribution of cardiomyocytes, indicates a high degree of consistency and reliability in the measurements obtained from the platform. This uniformity is further supported by the similarity in the initial offsets of the strain sensors patterned on the device, which is a crucial factor in enhancing the platform's reliability.

This study further explored the efficacy of a novel cantilever-based platform designed to assess the impacts of pharmacological agents on cardiomyocytes. We examined the response of these cardiomyocytes to a diverse group of drugs: Nifedipine (a Ca^{2+} channel blocker), Bay K-8644 (a Ca^{2+} channel activator), Astemizole (a K^+ channel blocker), Quinidine (a Na^+ channel blocker), Blebbistatin (a myosin inhibitor), and Isoproterenol (a beta adrenoceptor). These agents, as detailed in Table S1 (Supporting Information), modulate electrophysiological and contractile properties of cardiomyocytes in distinct ways. Specifically, ion channel blockers generally induced negative chronotropy and inotropy, with varied effects on FPD and field potential amplitude (FPA).

A key finding of this work is the differentiation in the impact of these drugs on the electrophysiological and mechanical properties of cardiomyocytes. Our data suggest that this multifunctional platform could be instrumental in the drug toxicity screening process, especially for novel compounds. We observed that the ion channel blockers altered FPD in response to increasing drug concentrations, simultaneously affecting contraction force and beat rate. Intriguingly, the toxicity profiles of these drugs, as measured by their half-maximal inhibitory con-

centration (IC_{50}), varied across different parameters. Traditional methods of drug-induced toxicity screening primarily focus on the IC_{50} of the APD; however, our study highlights the limitations of this approach, particularly for drugs that do not block the hERG channel. We demonstrated these limitations and the potential of our platform using several drugs, including Nifedipine, Bay K-8644, Isoproterenol, and Blebbistatin. For instance, Nifedipine showed a marked difference in IC_{50} values when assessed for FPD and contractility. When evaluating the toxicity of Blebbistatin, using electrophysiology as a measure is not feasible due to its direct impact on contractile mechanisms. At $10\text{ }\mu\text{M}$ concentrations of Blebbistatin, although cardiac electrophysiological signals remain strong enough, the beating of cardiomyocytes had completely stopped. These findings underscore the importance of evaluating contractile IC_{50} alongside electrophysiological metrics, as it provides a more comprehensive understanding of drug-induced cardiotoxicity.

Moreover, our study emphasizes the need for a holistic approach to cardiotoxicity assessment, integrating both electrophysiological and contractile measurements. The role of contraction force as a reliable marker of drug toxicity is particularly highlighted, given its sensitivity to intracellular changes and its connection to critical cellular processes involving Ca^{2+} and other proteins. While there are existing platforms for simultaneous electrical and mechanical screening of cardiomyocytes, our study is unique in its in-depth analysis and demonstration of the necessity for such comprehensive assessments. The limitations of standalone electrophysiological screening, as evidenced by the behaviors of drugs like Nifedipine, Bay K-8644, Blebbistatin, and Isoproterenol, further reinforce the value of our multifaceted approach in drug toxicity screening.

4. Conclusion

In this research, we developed a multifunctional device and platform capable of simultaneously measuring the contraction force and field potential of different cardiac tissue samples on 8 different cantilevers. This capability is achieved by integrating the cantilevers with strain sensors and 64 microelectrodes. Our strain sensors demonstrate remarkable sensitivity, capable of detecting forces as small as $2\text{ }\mu\text{N}$ caused by cardiac tissue activity. In addition, the conductive layer and microgroove patterns on the cantilevers significantly enhance tissue maturation and interconnectivity, as indicated by distinct protein expression patterns. A notable finding in our study pertains to the experimental results of drug toxicity screening. We observed that traditional methods focusing primarily on the half-maximal inhibitory concentration (IC_{50}) of FPD inadequately represent the complexity of drug-induced cardiotoxicity. Our platform uniquely illustrates the different impacts of various drugs on the electrophysiological and mechanical properties of cardiomyocytes. This dual assessment approach, employing both MEA and strain sensors, provides a more comprehensive and nuanced understanding of cardiotoxic effects. This is particularly crucial for drugs that do not primarily target the hERG channel. The use of our proposed integrated methodology is expected to provide a deeper understanding of the mechanisms of cardiac toxicity and help in the development of safer medicines for the heart.

5. Experimental Section

Fabrication of the Multifunctional Cantilever-Based Device: The fabrication process of the cantilever until the patterning of microgrooves was carried out as described by Kanade et al.^[39] in which the authors fabricated a non-conductive SU-8 based cantilever. Briefly, the device was created using standard photolithographic methods. It was built on a silicon wafer coated with a 300 nm silicon dioxide layer, achieved through wet oxidation. This base was necessary since SU-8, a photosensitive polymer used in the process, would be ultimately released from the sacrificial oxide layer. For patterning the MEA, internal reference electrode, strain sensor and laser reflection area, a Ti/Au layer with a thickness of 10/100 nm was utilized. An isolation layer $\approx 1 \mu\text{m}$ thick was then designed using SU-8, specifying the exposed area of MEA and insulating the associated wires and strain sensor. A 4×2 array, featuring a $50 \mu\text{m}$ diameter MEA with a $350 \mu\text{m}$ pitch, was organized on the cantilever. SU-8 was also used to create microgrooves with a $3 \mu\text{m}$ width and pitch. Subsequently, an e-beam patterned a Ti/Au conductive layer on the cantilever, excluding the MEA section. To ensure the metal pattern remained intact during extended immersion in buffered oxide etchant (6:1) (BOE) during the final stage, the edges of this conductive layer were protected with SU-8 2002. Once the edges were safeguarded, the body layer was crafted using SU-8 2050, following the procedure outlined in Kanade et al. (2022).^[39] The final step involved detaching the device from the silicon dioxide layer using BOE. The detailed fabrication steps for the device are illustrated in Figure S20a (Supporting Information).

To connect the strain sensor and MEA electrical contacts with a PCB for data acquisition, the polymer cantilever body was first connected to a customized $4 \text{ cm} \times 4 \text{ cm}$ glass slide (Figure S20b, Supporting Information). Before bonding, the glass was patterned with metal contacts made of Ti/Au using previously described metal patterning protocol. A $20 \mu\text{m}$ layer of Perminex 1010 was then spin coated on the patterned glass at 500 rpm for 10 s and 1000 rpm for 30 s. Perminex is a photosensitive negative epoxy photoresist that was used for bonding the cantilever body with that of the glass. The Perminex layer was soft baked at 95°C for 30 min and let it cool down. It was then exposed to UV at 900 mJ cm^{-2} under a custom-patterned mask. Upon post exposure baking at 70°C for 2 min, the pattern was developed in PN1000 developed for ≈ 10 min and then rinsed with fresh developer for ≈ 1 min. The bonding of the cantilever body and the patterned glass was carried out at an elevated temperature of 150°C for 30 s at 1.6 kN pressure. Thereafter, conductive epoxy was used to bond the contact pads on the device with those on glass. This prepared device was then glued to the custom-made PCB and contacts were bonded using a wire-bonder. The design and wiring diagram of the custom-made PCB is shown in Figure S21 (Supporting Information). The culture ring and PCB connectors were then connected, and the device was ready for cell culture.

Design of the Integrated Platform for Simultaneous Measurement of Cardiac Field Potential and Contractility: The integrated universal platform for the simultaneous measurement of field potential and contractility was designed as shown in Figure 1d, with the device in the stage-top incubator (Live Cell Instrument, Chamlyde WP) (Figure S2a, Supporting Information) and the allied setup in the system enclosure (Figure S2b, Supporting Information). Inside the enclosure, the bottom most layer was placed for AC-DC power supply (Powerplaza, NFT30-5FFA) with three outputs (+5 V/+15 V/-15 V) and the DAQ USB 6001 (Figure S3a, Supporting Information). The 5 VDC was to power up the MEA interface board while the +15 Vdc and -15 Vdc were to be supplied to the strain sensor filter and amplifier circuits. The second layer of the system enclosure consisted of the filter and amplifier circuit for the eight strain sensors (Figure S3b, Supporting Information). The filter circuit was designed for the 3rd order active filter using OPA2277 and the amplifier using INA118. The circuit diagram of this design is shown in Figure S22 (Supporting Information). The third layer was designed to place the MEA interface board (Intan technologies, RHD2000) with the RHD2164 64-channel headstage connected directly to the device PCB in the stage-top incubator (Figure S3c, Supporting Information). A custom-made PCB was designed for the connection of RHD2164 with the device (Figure S23, Supporting Information). In the system, a commercial setup was used for the MEA data handling, while

the strain sensor measurement was carried out using the custom-made circuit.

For data acquisition and storage, the MEA data was handled by the official open-source software by Intan technologies, while a custom-built Lab-View program was designed for the strain sensor.

Characterization of the Strain Sensor and MEA: *Characterization of the Strain Sensor for its Minimum Detection:* The strain sensor amplifier was characterized for detecting the minimum limit of the cantilever. An automated Z-stage was used to precisely control the deflection of the cantilever. The data was converted to the digital format using DAQ.

Characterization of the MEA for its Base Impedance: The field potential was recorded utilizing the RHD2164 headstage and RHD2000 USB interface board from Intan technologies. Using the 3-electrode technique, the base impedance of MEA was determined. The designed microelectrodes functioned as the active electrode, while Ag/AgCl and Pt acted as the reference and counter electrodes, in that order. The electrolyte solution chosen for this process was phosphate buffered saline (PBS). Impedance evaluation was conducted using the CompactStat from IVIUM Technologies (Standard type, Eindhoven, The Netherlands), applying a potential of 10 mV.

The protocols for NRVM cell culture and Western blot are described in the supplementary information.

Simultaneous Measurement of Contraction Force and Field Potential of Cardiomyocytes: The force of contraction by the cardiomyocytes was quantified through the voltage output from the strain sensor using the developed signal conditioning unit and a tailor-made DAQ consisting of NI DAQ USB 6001 combined with LabView software. Concurrently, the field potential from the MEA was captured using Intan technologies' commercial setup, specifically employing the Intan RHD interface board and the 64-channel RHD2164 headstage. All simultaneous measurements were carried out between day 11 and day 14 after cell culture.

Drugs Toxicity Screening Protocol: Six drugs were used in this work – Quinidine, Nifedipine, Astemizole, Isoproterenol, Bay K-8644 and Blebbistatin. All the drugs were purchased from Sigma Aldrich and the stock solution was prepared in dimethyl sulfoxide (DMSO). Drug concentrations were added sequentially in the culture media with the maximum DMSO concentration of 0.12%, and the waiting period between each dose was 15 min.

Characterization of Field Potential and Contractile Parameters and Statistical Analysis: The field potential duration (FPD), contraction-relaxation duration (CRD), rise time, decay time, beat rate, and contraction force were characterized near IC_{50} with respect to control. All durations corrected by Fredericia's equation: Corrected duration = Duration (interspike interval)^{-1/3}. Field potential data were analyzed in MATLAB using custom-made algorithms. Contractility analyses were conducted on unsmoothed profiles. The results obtained are presented as mean \pm standard error of mean (S.E.M.). Drug toxicity screening was carried out on $n = 3$ biologically independent samples. Statistical significance of data was determined with the help of one-way ANOVA followed by Tukey's honest significant difference test with the help of GraphPad Prism 9, with significant differences defined by $*p < 0.05$ and $**p < 0.01$.

Supporting Information

Supporting Information is available from the Wiley Online Library or from the author.

Acknowledgements

This work was supported by the National Research Foundation of Korea (NRF) grant funded by the Korea government (MSIT) (No. RS-2022-00165505 and No. 2020R1A5A8018367). Authors would like to thank Dr. Yun-jin Jeong for his support during fabrication of the PCB, Dr. Dong-Su Kim for his support in the strain sensor pattern, and Mr. Longlong Li and Mr. Wang Lei for their help during development of the drug toxicity evaluation platform.

Conflict of Interest

The authors declare no conflict of interest.

Data Availability Statement

The data that support the findings of this study are available from the corresponding author upon reasonable request.

Keywords

arrhythmia, cantilever, cardiomyocytes, contractility, field potential, micro-electrode array, strain sensor

Received: December 5, 2023

Revised: March 8, 2024

Published online:

- [1] N. S. Craveiro, B. S. Lopes, L. Tomás, S. F. Almeida, *Curr Drug Saf* **2019**, 15, 4.
- [2] O. J. Wouters, M. McKee, J. Luyten, *JAMA – Journal of the American Medical Association* **2020**, 323, 844.
- [3] R. L. Martin, Z. Su, J. T. Limberis, J. D. Palmatier, M. D. Cowart, B. F. Cox, G. A. Gintant, In Vitro Preclinical Cardiac Assessment of Tolterodine and Terodiline: Multiple Factors Predict the Clinical Experience.
- [4] M. Uchikawa, M. Hashiguchi, T. Shiga, *Drugs Real World Outcomes* **2022**, 9, 551.
- [5] R. M. Lester, J. Olbertz, *Expert Rev. Clin. Pharmacol.* **2016**, 9, 1611.
- [6] S. Peng, A. E. Lacerda, G. E. Kirsch, A. M. Brown, A. Bruening-Wright, *J. Pharmacol. Toxicol. Methods* **2010**, 61, 277.
- [7] E. S. Richardson, Y.-F. Xiao, *Cardiac Electrophysiology methods and models*, Springer, Berlin, **2010**, 329.
- [8] E. G. Navarrete, P. Liang, F. Lan, V. Sanchez-Freire, C. Simmons, T. Gong, A. Sharma, P. W. Burridge, B. Patlolla, A. S. Lee, H. Wu, R. E. Beygui, S. M. Wu, R. C. Robbins, D. M. Bers, J. C. Wu, *Circulation* **2013**, 128, S3.
- [9] A. S. T. Smith, E. Choi, K. Gray, J. Macadangdang, E. H. Ahn, E. C. Clark, M. A. Laflamme, J. C. Wu, C. E. Murry, L. Tung, D. H. Kim, *Nano Lett.* **2020**, 20, 1561.
- [10] M. D. Halbach, U. Egert, J. Hescheler, K. Banach, *Cell. Physiol. Biochem.* **2003**, 13, 271.
- [11] Y. Asahi, T. Hamada, A. Hattori, K. Matsuura, M. Odaka, F. Nomura, T. Kaneko, Y. Abe, K. Takasuna, A. Sanbuissho, K. Yasuda, *Sci Rep* **2018**, 8, 14536.
- [12] H. M. Himmel, A. Bussek, M. Hoffmann, R. Beckmann, H. Lohmann, M. Schmidt, E. Wettwer, *Br. J. Pharmacol.* **2012**, 166, 276.
- [13] S. P. Wells, H. M. Waddell, C. Boon Sim, X. Y. Shiang Lim, G. B. Bernasocchi, X. Davor Pavlovic, P. Kirchhof, E. R. Porrello, L. M. D. Delbridge, J. R. Bell, D. Lmd, *Am. J. Physiol. Cell Physiol.* **2019**, 317, C1256.
- [14] J. Fang, Y. Pan, J. Xu, D. Xu, H. Li, C. Liu, N. Hu, *Nano Lett.* **2023**, 23, 4049.
- [15] J. Fang, D. Xu, H. Wang, J. Wu, Y. Li, T. Yang, C. Liu, N. Hu, *Nano Lett.* **2023**, 23, 243.
- [16] Y. Xiang, H. Liu, W. Yang, Z. Xu, Y. Wu, Z. Tang, Z. Zhu, Z. Zeng, D. Wang, T. Wang, N. Hu, D. Zhang, *Microsyst Nanoeng* **2022**, 8, 70.
- [17] M. Dipalo, S. K. Rastogi, L. Matino, R. Garg, J. Bliley, G. Iachetta, G. Melle, R. Shrestha, S. Shen, F. Santoro, A. W. Feinberg, A. Barbaglia, T. Cohen-Karni, F. De Angelis, Intracellular Action Potential Recordings from Cardiomyocytes by Ultrafast Pulsed Laser Irradiation of Fuzzy Graphene Microelectrodes, **2021**.
- [18] C. Antzelevitch, A. Burashnikov, S. Sicouri, L. Belardinelli, *Heart Rhythm* **2011**, 8, 1281.
- [19] C. T. January, J. M. Riddle, J. J. Salata, A Model for Early Afterdepolarizations: Induction With the Ca²⁺ Channel Agonist Bay K 8644.
- [20] V. Kappadan, S. Telele, I. Uzelac, F. Fenton, U. Parltitz, S. Luther, J. Christoph, *Front Physiol* **2020**, 11, 464.
- [21] Y. Dou, P. Arlock, A. Arner, *Am. J. Physiol. Cell Physiol.* **2007**, 293, C1148.
- [22] U. Saleem, I. Mannhardt, I. Braren, C. Denning, T. Eschenhagen, A. Hansen, *Stem Cell Rep.* **2020**, 14, 312.
- [23] K. J. Hansen, J. T. Favreau, J. R. Gershlak, M. A. Laflamme, D. R. Albrecht, G. R. Gaudette, *Tissue Eng Part C Methods* **2017**, 23, 445.
- [24] D. M. Bers, *Annu. Rev. Physiol.* **2008**, 70, 23.
- [25] W. D. Gao, N. G. Perez, E. Marban, *Journal of Physiology* **1998**, 507, 175.
- [26] D. M. Bers, in *Cardiac Electrophysiology: From Cell to Bedside: Sixth Edition*, Elsevier Inc., New York, **2014**, pp. 161–169.
- [27] G. Caluori, J. Pribyl, M. Pesl, S. Jelinkova, V. Rotrekl, P. Skladal, R. Raiteri, *Biosens. Bioelectron.* **2019**, 124–125, 129.
- [28] J. F. S. Cogollo, M. Tedesco, S. Martinoia, R. Raiteri, *Biomed. Microdevices* **2011**, 13, 613.
- [29] T. Hayakawa, T. Kunihiro, T. Ando, S. Kobayashi, E. Matsui, H. Yada, Y. Kanda, J. Kurokawa, T. Furukawa, *J. Mol. Cell. Cardiol.* **2014**, 77, 178.
- [30] J. Fang, X. Wei, H. Li, N. Hu, X. Liu, D. Xu, T. Zhang, H. Wan, P. Wang, X. Xie, *Microsyst Nanoeng* **2021**, 7, 26.
- [31] N. Hu, T. Wang, H. Wan, L. Zhuang, R. Kettenhofen, X. Zhang, Y. S. Zhang, W. Xu, M. Gossmann, H. Bohlen, X. Hou, P. Wang, *Biosens. Bioelectron.* **2018**, 117, 354.
- [32] H. Li, J. Fang, X. Wei, D. Xu, T. Zhang, Y. Xiang, H. J. Chen, F. Liu, X. Xie, P. Wang, N. Hu, *Biosens. Bioelectron.* **2020**, 162, 112273.
- [33] N. E. Oyunbaatar, Y. Dai, A. Shanmugasundaram, B. K. Lee, E. S. Kim, D. W. Lee, *ACS Sens.* **2019**, 4, 2623.
- [34] F. Qian, C. Huang, Y. D. Lin, A. N. Ivanovskaya, T. J. O'Hara, R. H. Booth, C. J. Creek, H. A. Enright, D. A. Soscia, A. M. Belle, R. Liao, F. C. Lightstone, K. S. Kulp, E. K. Wheeler, *Lab Chip* **2017**, 17, 1732.
- [35] X. Wei, D. Jiang, C. Chen, J. Wu, C. Qin, Q. Yuan, Y. Xue, Y. Xiong, L. Zhuang, N. Hu, P. Wang, *ACS Sens.* **2021**, 6, 2593.
- [36] T. Ohya, H. Ohtomo, T. Kikuchi, D. Sasaki, Y. Kawamura, K. Matsuura, T. Shimizu, K. Fukuda, T. Someya, S. Umezaki, *Lab Chip* **2021**, 21, 3899.
- [37] Z. Zhao, Y. J. Jeong, N. E. Oyunbaatar, R. B. Pujari, P. P. Kanade, E. S. Kim, B. K. Lee, D. W. Lee, *Sens Actuators B Chem* **2022**, 358, 131495.
- [38] W. Dou, M. Malhi, T. Cui, M. Wang, T. Wang, G. Shan, J. Law, Z. Gong, J. Plakhotnik, T. Filleter, R. Li, C. A. Simmons, J. T. Maynes, Y. Sun, *ACS Nano* **2022**, 16, 11278.
- [39] P. P. Kanade, N. E. Oyunbaatar, A. Shanmugasundaram, Y. J. Jeong, E. S. Kim, B. K. Lee, D. W. Lee, *Biosens. Bioelectron.* **2022**, 216, 114675.
- [40] J. Kim, A. Shanmugasundaram, D. W. Lee, *Analyst* **2021**, 146, 6768.
- [41] M. Hopcroft, T. Kramer, G. Kim, K. Takashima, Y. Higo, D. Moore, J. Brugger, *Fatigue Fract. Eng. Mater. Struct.* **2005**, 28, 735.
- [42] C. Oleaga, G. Legters, L. R. Bridges, L. Kumanchik, C. Martin, Y. Cai, M. Schnepfer, C. W. McAleer, C. J. Long, J. J. Hickman, *Contractile Force Readout of hESC-Cardiomyocytes*, **2017**, pp. 229–246.
- [43] K. Wilson, M. Das, K. J. Wahl, R. J. Colton, J. Hickman, *PLoS One* **2010**, 5, e11042.
- [44] D. S. Kim, Y. J. Jeong, J. Park, A. Shanmugasundaram, D. W. Lee, *Analyst* **2021**, 146, 7160.
- [45] O. Sensch, W. Vierling, W. Brandt, M. Reiter, *Br. J. Pharmacol.* **2000**, 131, 1089.
- [46] C. Larsson-Backström, E. Arrhenius, K. Sagge, *Acta Pharmacol Toxicol (Copenh)* **1985**, 57, 8.
- [47] G. M. Wahler, N. Sperelakis, New Ca²⁺ Agonist (Bay K 8644) Enhances and Induces Cardiac Slow Action Potentials, **1984**.
- [48] G. Thomas, M. Chung, C. J. Cohen, A Dihydropyridine (Bay k 8644) That Enhances Calcium Currents in Guinea Pig and Calf Myocardial Cells A New Type of Positive Inotropic Agent.

- [49] C. T. January, J. M. Riddle, J. J. Salata, A Model for Early Afterdepolarizations: Induction With the Ca²⁺ Channel Agonist Bay K 8644.
- [50] Z. Zhou, V. R. Vorperian, Q. Gong, S. Zhang, C. T. January, *J Cardiovasc Electrophysiol* **1999**, 10, 836.
- [51] A. Sugiyama, N. Aye, Effects of Nonsedating Antihistamine, Astemizole, on Thein SituCanine Heart Assessed by Cardiohemodynamic and Monophasic Action Potential Monitoring Halothane-Anesthetized Canine Model View Project IPS Derived Cardiomyocytes View Project, **1997**.
- [52] J. Vicente, L. Johannesen, J. W. Mason, W. J. Crumb, E. Pueyo, N. Stockbridge, D. G. Strauss, *J Am Heart Assoc* **2015**, 4, 1615.
- [53] F. Sahli Costabal, J. Yao, E. Kuhl, *Int J Numer Method Biomed Eng* **2018**, 34, 2964.
- [54] J. Limouze, A. F. Straight, T. Mitchison, J. R. Sellers, Specificity of Blebbistatin, an Inhibitor of Myosin II.
- [55] K. S. Ginsburg, D. M. Bers, *Journal of Physiology* **2004**, 556, 463.